J Fluoresc (2007) 17:444–451
DOI 10.1007/s10895-007-0191-3

ORIGINAL PAPER

Comparative Investigation on Nanocrystal Structure and Luminescence Properties of Gadolinium Molybdates Codoped with Er^{3+}/Yb^{3+}

Y. X. Pan · Q. Y. Zhang · Z. H. Jiang

Received: 12 December 2006 / Accepted: 3 April 2007 / Published online: 18 May 2007

Abstract This paper reports on the comparative investigation of nanocrystal structure and luminescence properties of Er^{3+}/Yb^{3+}-codoped gadolinium molybdate nanocrystals $Gd_2(MoO_4)_3$ and Gd_2MoO_6 synthesized by the Pechini method with citric acid and ethylene glycol. Their crystallization, structure transformation, and morphologies have been investigated by X-ray diffraction, thermogravimetric/differential scanning calorimetry, and transmission electron microscopy. It is noticed that Er^{3+}/Yb^{3+}-codoped monoclinic $Gd_2(MoO_4)_3$ nanocrystals have shown an intense upconversion through a sintering of the organic complex precursor at 600°C. Furthermore, it transforms to orthorhombic $Gd_2(MoO_4)_3$ when the precursor is sintered at 900°C. In counterpart of monoclinic Gd_2MoO_6, however, the monoclinic structure remains unchanged when the precursor is sintered at a temperature ranging from 600°C to 900°C. Intense visible emissions of Er^{3+} attributed to the transitions of $^2H_{11/2}$, $^4S_{3/2}$–$^4I_{15/2}$ at 520 and 550 nm, and $^4F_{9/2}$–$^4I_{15/2}$ at 650 nm have been observed upon an excitation with a UV source and a 980 nm laser diode, and the involved mechanisms have been explained. It is quite interesting to observe obvious differences both in the excitation and the upconversion emission spectra of Er^{3+}/Yb^{3+}-codoped $Gd_2(MoO_4)_3$ respectively with monoclinic and orthorhombic structure. The quadratic dependence of fluorescence on excitation laser power has confirmed that two-photons contribute to upconversion of the green–red emissions.

Keywords Nanophosphor · Gadolinium molybdate · Upconversion luminescence

Y. X. Pan · Q. Y. Zhang (✉) · Z. H. Jiang
Key Lab of Specially Functional Materials of Ministry of Education and Institute of Optical communication, South China University of Technology, Guangzhou 510641, People's Republic of China
e-mail: qyzhang@scut.edu.cn

Y. X. Pan · Z. H. Jiang
College of Chemistry, South China University of Technology, Guangzhou 510641, People's Republic of China

Introduction

Over the past several years, rare earth ion doped nanocrystals have attracted a considerable attention for their fascinating optical properties compared to bulk materials and their potential applications in lighting and display. [1–4] In particular, Er^{3+} doped infrared-to-visible upconversion luminescent (UL) materials have extensively been investigated for various applications such as display, infrared inspection and pretending, and optical storages, thanks to the availability of high-power laser diodes (LD) [5–10]. Recently, nanosized UL materials have been found to be a good biological probe in immunoassaying, diagnosing, and therapy by tracking and determination the locations of biological molecules such as DNA, RNA, and protein [11, 12]. Crystallized UL particles as small as possible are required to be dispersed in a solution and form a stable suspension since the joint reaction between biochip and DNA molecules are often realized in a solution [13, 14]. The excitation wavelength at 980 nm is outside the luminescent absorption range of biological molecules, which is favorable for deeper penetration of excitation, easy escape of emitted light, and minimizing deleterious effects on biomaterials [15].

UL was observed in some Er^{3+} doped oxides, such as Gd_2O_3 [5, 6], Y_2O_3 [7, 8], ZrO_2 [9], fluorides [12], and lanthanum molybdate [18, 19]. It was reported that the

sharp decrease of the UL intensity of the Er^{3+} doped lanthanum molybdate was due to the formation of bulk materials at 1,000°C [18]. However, the influence of phase transformation of Er^{3+} doped tetragonal lanthanum molybdate on UL intensity at a high temperature should have been considered. It is well documented that single crystals of gadolinium molybdate $Gd_2(MoO_4)_3$ possessing mixed ferroelastic and ferroelectric properties have been applied in electric and mechanical field [20, 21]. By far, however, the photoluminescence of rare earth ions doped gadolinium molybdates with different structures has not systematically been investigated.

To obtain desired rare earth ions doped luminescent nanocrystals, wet chemistry such as sol-gel method [4, 5, 9], hydrothermal synthesis [6, 12], combustion [7], coprecipitation [8], and the Pechini method [16, 17, 22], at a relatively low temperature, have been extensively adopted. The starting materials in these methods can be mixed at molecular-level and the temperature for nanocrystal crystallization is relatively lower than that needed in the solid state method. It is worthy to note that the Pechini method is based on the polyesterification between citric acid and ethylene glycol and producing nanomaterials at a low temperature [16, 17]. Metal atoms are dispersed and mixed uniformly in a rigid polyester network. The size of nanocrystal could be tailored by sintering the precursors at different temperatures but the structure of nanocrystals remains unchanged [22].

The main objective of this work is to carry out a detailed study on the nanocrystal structure and luminescence properties of Er^{3+}/Yb^{3+}-codoped gadolinium molybdates with high upconversion efficiency, chemical and physical stableness, and sensitivity for potential application in bioassays. It is the first time that Er^{3+} and Yb^{3+} codoped gadolinium molybdate nanocrystals with different structures have been synthesized by means of the Pechini method.

Experimental section

Synthesis of Er^{3+} and Yb^{3+} codoped gadolinium molybdate nanocrystals

Rare earth oxides Gd_2O_3 (99.99%), Er_2O_3 (99.99%), Yb_2O_3 (99.99%) were dissolved in HNO_3 (A.R.) to form rare earth nitrates solutions. To prepare the mixture solution of ammonium molybdate and organic components, ammonium molybdate $(NH_4)_2MoO_4$ (A.R.) and citric acid (A.R.) were dissolved in mixture solvent of ethylene glycol (A.R.) and distilled water. The previously prepared rare earth nitrates solutions were added dropwise to the mixed solution of ammonium molybdate and organic components with a molar ratio of (2-*x*-*y*) Gd^{3+}: xEr^{3+}: yYb^{3+}: 3 $[MoO_4]^{2-}$ for sample $Gd_2(MoO_4)_3$:Er^{3+}, Yb^{3+} and (2-*x*-*y*) Gd^{3+}: xEr^{3+}: yYb^{3+}: $[MoO_4]^{2-}$ for Gd_2MoO_6:Er^{3+}, Yb^{3+} (x=0.01, 0.02, 0.04, 0.06, 0.1, 0.14, 0.18 and 0. 22; y=0, 0.1, 0.2, 0.3, 0.4, 0.6 and 0.8) respectively. The mixture was then heated in an induction heating plate with temperature range from 100–250°C for 10 min with vigorous stirring. The solution was concentrated by evaporating the solvent, and its color changed from a pale yellow to a bright yellow, and then to a brown. After further heating, a dark ash-like solid was achieved. Ultrafine white gadolinium molybdate UL powders were obtained by sintering the precursors at above 600°C for 5 h.

Characterization

The crystallization and phase transformation behavior of gadolinium molybdates were monitored by both thermogravimetric analysis (TGA)/different scanning calorimeter (DSC; Netzsch STA 449C, at a heating rate of 10 K/min) and X-ray diffraction (XRD; Philips Model PW1830 diffractometer, Cu $K\alpha$). Transmission electron microscope (TEM; JEM-1010 electron microscope) was used to characterize the morphology of gadolinium molybdates. Room temperature excitation and emission spectra of the samples were recorded on a TRIAX320 spectrofluorimeter (Jobin-Yvon, France) with xenon and 980 nm LD as excitation sources. Emitted light was focused onto the monochromator and was monitored at the exit slit by a photon-counting R5108 photomultiplier tube and InGaAs detector for light in the visible and infrared region respectively.

Results and discussion

Structural and morphological characterization

The thermal decomposition of the precursors of $Gd_2(MoO_4)_3$ (G1) and Gd_2MoO_6 (G2) in the Pechini method could be roughly divided into three stages according to the TGA/DSC curves as shown in Fig. 1. We confirm the weight loss of about 5% in the first stage at the temperature lower than 205°C is mainly attributed to the adsorbed moisture since a weak endothermic peak presents in DSC curves in this temperature range. The speed of weight loss arrives at the maximum shown in DSC curves and the total weight loss arrives at 43% at about 736°C in the second stage as shown in both TG curves. In this stage, the strong exothermic peak at 284°C in the DSC curve of G1 and two strong exothermic peaks at 380 and 458°C in that of G2 are due to the combustion of the organic components such as citric acid, citrate, and ethylene glycol. Also, in the third stage, an intense exothermic peak at 726°C presents in DSC curve accompanied with further weight loss in TG curve of G1,

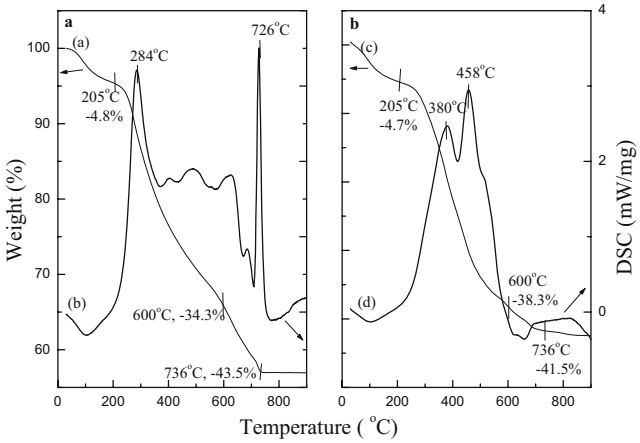

Fig. 1 TG-DSC graphs of the precursors of **a** $Gd_{1.78}Yb_{0.2}Er_{0.02}(MoO_4)_3$ and **b** $Gd_{1.78}Yb_{0.2}Er_{0.02}MoO_6$

which is due to the structural transformation of G1 crystals. In the counterpart of G2, a strong exothermic peak is not observed in the DSC curve and the trend of weight loss of the TG curve becomes slow at a temperature higher than 681°C. This indicates that the combustion of the organic components has been completed and no phase transition occurred in G2. The results will be further confirmed by XRD patterns in the next section.

Figure 2b shows that 500°C is not high enough to remove organic components and crystallize nanocrystals. Pure monoclinic $Gd_2(MoO_4)_3$ (m-G1) phase with space group C2/c (15), which is in good agreement with JCPDS Card (No. 25-0338; Fig. 2a), is achieved by sintering the G1 precursor at 600°C (Fig. 2c). The orthorhombic $Gd_2(MoO_4)_3$ (o-G1) phase accompanied with a small

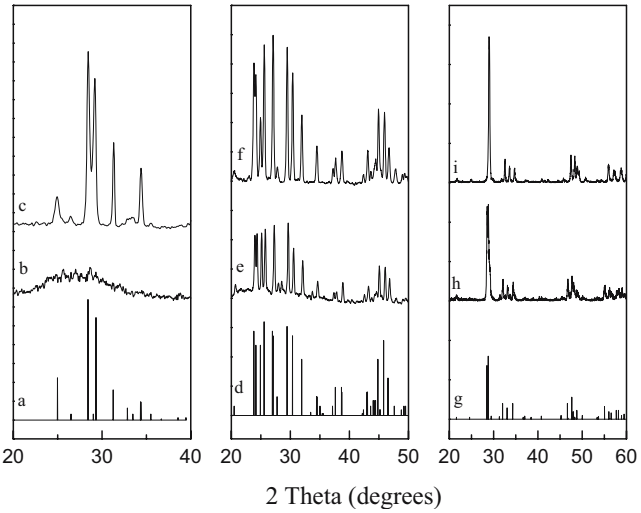

Fig. 2 XRD of the Er^{3+} and Yb^{3+} codoped gadolinium molybdate nanocrystals obtained by sintering the precursor of $Gd_{1.78}Yb_{0.2}Er_{0.02}(MoO_4)_3$ at *b* 500°C, *c* 600°C, *e* 800°C, *f* 900°C; and by sintering the precursor of $Gd_{1.78}Yb_{0.2}Er_{0.02}MoO_6$ at *h* 600°C, *i* 900°C; JCPDS Cards of monoclinic $Gd_2(MoO_4)_3$, orthorhombic $Gd_2(MoO_4)_3$ and monoclinic Gd_2MoO_6 are shown as *a*, *d*, and *g* respectively

quantity of m-G1 is obtained at 800°C (Fig. 2e). Pure phase o-G1 with space group of Pba2 (32) matching well with JCPDS Card (No. 2520-0408; Fig. 2d) is achieved at 900°C (Fig. 2f) and it is ascribed due to a negative thermal expansion from monoclinic to orthorhombic structure with a temperature rise [23]. The phase transformation indicated in XRD pattern is in accordance with an exothermic process in DSC curve of the precursor of G1 in Fig. 1b. Single phase monoclinic Gd_2MoO_6 (m-G2) with space group 12/a (15) matched well with JCPDS Card (No. 24-0423; Fig. 2g) is obtained by sintering the G2 precursor at 600 and 900°C (Fig. 2h,i). Stoichiometric doping Yb^{3+} and Er^{3+} has a negligible influence on the resultant structure which is due to the similarity of the ion radii and also due to existence of the equal electric charges between Gd^{3+} and dopants Yb^{3+} and/or Er^{3+}.

In Fig. 3, Low magnification TEM images show that as-prepared gadolinium molybdate nanocrystals are of uniform sphere-like shape, with narrow size distribution and mean sizes in the range from 50–70 nm. This is larger than calculated from Debye-Scherre's equation indicating that these particles are composed of nanosized polycrystalline. High-resolution TEM (HRTEM) images of the nanoparticles show well-resolved and clear fringes demonstrating complete crystallinity of these nanoparticles. The selected area electron diffraction patterns further demonstrate that the as-prepared gadolinium molybdate nanocrystals are polycrystalline.

Luminescence properties

Luminescence spectra in visible region

The excitation spectra and the corresponding emission spectra of monoclinic $Gd_2(MoO_4)_3$:Er^{3+},Yb^{3+} (*m*-G1-YE), orthorhombic $Gd_2(MoO_4)_3$:Er^{3+},Yb^{3+} (o-m-G1-YE), and monoclinic Gd_2MoO_6:Er^{3+},Yb^{3+} (m-G2-YE) nanocrystals excited by xenon source are shown in Fig. 4. It should be noted that the luminescent intensities in the spectra of m-G2 have been magnified for the purpose of comparative investigation. The locations and shapes of the peaks in the excitation spectra of m-G1-YE and o-G1-YE are almost similar except that the peaks in former excitation spectrum are much more intense than those in later one. Three peaks at 365, 378, and 406 nm are attributed to the transitions from ground state $^4I_{15/2}$ to excited states $^4G_{7/2}$, $^4G_{11/2}$, $^2H_{9/2}$ of Er^{3+} directly excited by xenon source. In the region from 300 to 420 nm, no excitation peak is observed in the excitation spectra of m-G2-YE. The peak group at 450 nm is attributed to the transitions $^4I_{15/2}$–$^2F_{5/2,\ 3/2}$ and the intense excitation peaks at 487 nm are due to the transition $^4I_{15/2}$– $^2F_{7/2}$. The features of the three excitation curves indicate that Er^{3+} in m-G1 and o-G1 could be excited both at the UV wavelength

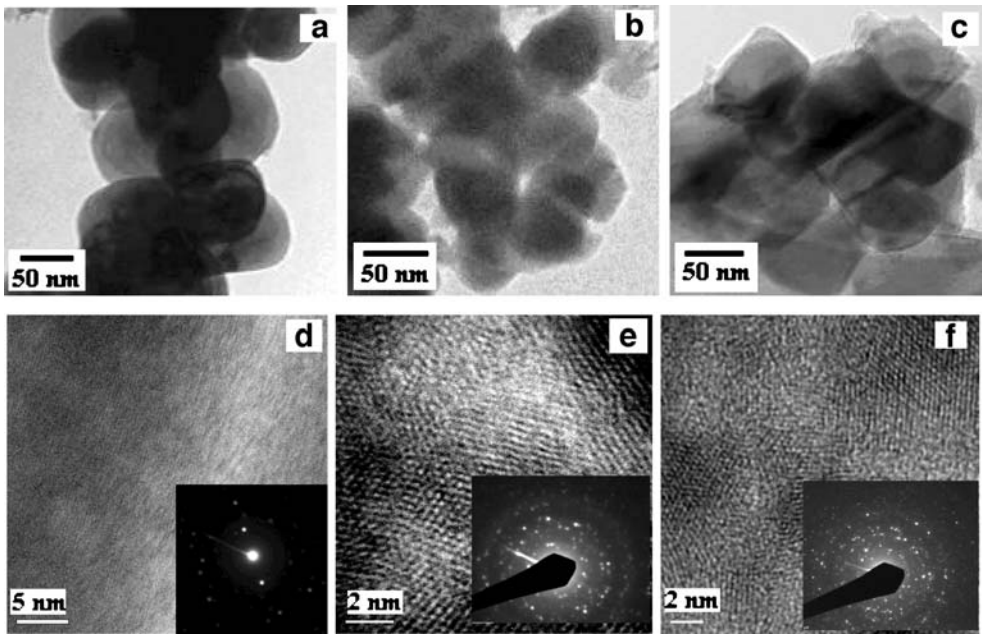

Fig. 3 TEM images of the **a** m-G1, **b** o-G1 and **c** m-G2 nanocrystals, and high-resolution TEM images of the nanocrystals: **d** m-G1, **e** o-G1, **f** m-G2 and the corresponding selected area electron diffraction pattern

378 nm and at the blue light of 488 nm, while Er^{3+} in G2 could only be efficiently excited by a blue light.

From the overall observation, an intense green emission accompanied with very weak red emission which are respectively originated from the transition $^2H_{11/2}$, $^4S_{3/2}$–$^4I_{15/2}$ and $^4F_{9/2}$–$^4I_{15/2}$ as shown in Fig. 4b. The multi-peaks of a transition are ascribed to the stark splitting of 4f states of Er^{3+} by the crystal field. It is interesting to note that the integrated emission intensity ratio of the transition $^2H_{11/2}$–$^4I_{15/2}$ to $^4S_{3/2}$–$^4I_{15/2}$ is 0.87 in m-G1-YE decreases to 0.39 in o-G2-YE. The luminescence intensities of Er^{3+} in m-G1-YE and o-G1-YE are obviously much higher than that in G2-YE.

Upconversion luminescence

Upconversion visible emissions are produced when excited with 980 nm LD through multiphoton absorption process including ground-state absorption (GSA), excited-state absorption (ESA), usually accompanied with non-radiative relaxation, and a multiphoton relaxation process (MRP). In Er^{3+} doped upconversion phosphors, the Er^{3+} ion is promoted from ground state $^4I_{15/2}$ to intermediate $^4I_{11/2}$ through GSA by absorption of one photon as depicted in the schematic energy level diagram in Fig. 10. The second photon promotes the Er^{3+} ion from $^4I_{11/2}$ to $^2F_{7/2}$ or from $^4I_{13/2}$ to $^4F_{9/2}$ through ESA. The populated level $^2F_{7/2}$

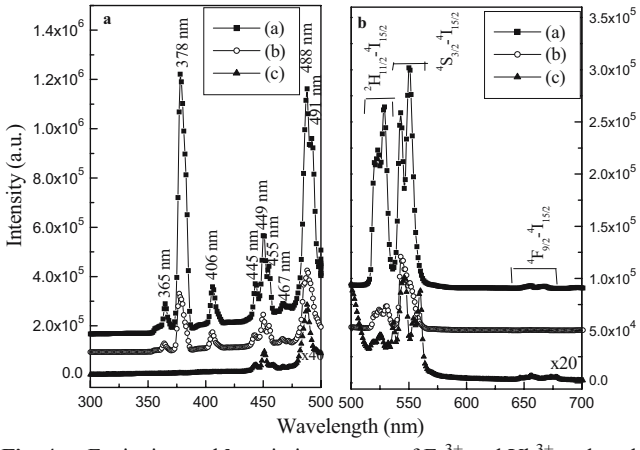

Fig. 4 **a** Excitation and **b** emission spectra of Er^{3+} and Yb^{3+} codoped (*a*) monoclinic $Gd_2(MoO_4)_3$ (λem=550 nm, λex=378 nm), (*b*) orthorhombic $Gd_2(MoO_4)_3$ (λem=550 nm, λex=378 nm), and (*c*) monoclinic Gd_2MoO_6 (λem=544 nm, λex=487 nm)

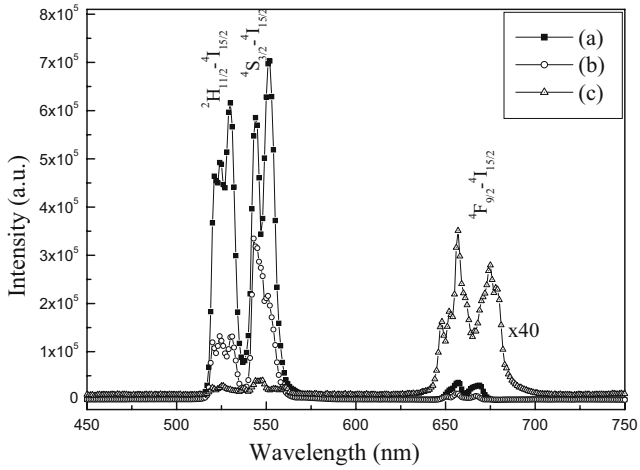

Fig. 5 **a** Upconversion luminescent spectra of Er^{3+} and Yb^{3+} codoped nanocrystals (*a*) monoclinic $Gd_2(MoO_4)_3$, (*b*) orthorhombic $Gd_2(MoO_4)_3$, (*c*) monoclinic Gd_2MoO_6 upon excitation at 980 nm with 38 mW

relaxes non-radiatively to $^2H_{11/2}$ due to narrow energy gaps between them. The processes are illustrated here:

$$\text{GSA}: Er^{3+}\left(^4I_{15/2}\right) + \text{a photon} \rightarrow Er^{3+}\left(^4I_{11/2}\right)$$

$$\text{ESA1}: Er^{3+}\left(^4I_{11/2}\right) + \text{a photon} \rightarrow Er^{3+}\left(^2F_{7/2}\right)$$

$$\text{ESA2}: Er^{3+}\left(^4I_{13/2}\right) + \text{a photon} \rightarrow Er^{3+}\left(^4F_{9/2}\right)$$

As shown in Fig. 5, a green emission at 550 nm and a red emission at 660 nm are produced by radiative transition of Er^{3+} ions from $^2H_{11/2}$ and $^4F_{9/2}$ to ground state $^4I_{15/2}$, respectively. The levels $^2H_{11/2}$ and $^4S_{3/2}$ with narrow gap of 800 cm^{-1} are in thermal equilibrium and MPR could occur consequently from $^2H_{11/2}$ to $^4S_{3/2}$. Radiative transition from $^4S_{3/2}$ to $^4I_{15/2}$ gives rise to intense emission at 520 nm. Quantitatively, the integrated emission intensity ratios of the transition $^4S_{3/2}$–$^4I_{15/2}$ to $^2H_{11/2}$–$^4I_{15/2}$ is 0.87 in the emission spectrum of m-G1-EY but 0.39 in that of o-G1-EY, which are in accordance with the results in Fig. 4. In addition, the integrated emission intensity ratios of green emission to red one (I_{red}/I_{green}) are 19.8, 27.9 and 0.115 for m-G1-YE, o-G1-YE and m-G2-YE respectively.

Pump power effects

In order to understand the involved mechanism how the excited states of $^2H_{11/2}$, $^4S_{3/2}$ and $^4F_{9/2}$ are populated, the dependence of UL intensity of these samples upon the pump power of LD are displayed in Fig. 6. An obvious increase of both red and green emissions with the pump power is observed due to promotion of the population in levels Er^{3+} ($^4I_{11/2}$) and Yb^{3+} ($^2F_{5/2}$). It is well established that the upconversion emission intensity (I_{UC}) is proportional to the n^{th} power of the intensity of IR excitation $\left(I_{IR}^n\right)$, where the integer n is the number of photons absorbed for per upconversion photon emitted. [24] A plot of $\log I_{UC}$ vs $\log\left(I_{IR}^n\right)$ yields a straight line with slope n. The values of n of green emissions are 1.74, 1.87, and 1.65 those of red emissions are 2.15, 1.84, and 2.13 for samples m-G1-YE, o-G1-YE and m-G2-YE respectively. These results indicate that either green or red emissions of these Er^{3+} and Yb^{3+} codoped gadolinium molybdate nanocrystals are originated due to a two-photon process as has been described in the previous paragraph. The Er^{3+} ion is excited into $^4I_{11/2}$ by absorption of one photon through GSA, and arrives at $^4F_{7/2}$ by absorption of second photon via ESA. Thus, the UL is produced when the excited ions could decay non-radiatively to the lower levels and subsequently transitions radiatively to ground state.

Luminescence spectra in IR region

The excitation spectra (monitored at 1,530 nm) and the infrared emission spectra (excited by 980 nm LD) of Er^{3+} and Yb^{3+} codoped gadolinium molybdates are presented in Fig. 7. The attributions of excitation peaks at the wavelength lower than 500 nm are similar to those when monitored at 550 nm as shown in Fig. 4a. The intense peaks at 523, 544, 658, 757 nm originate from the transitions $^4I_{15/2}$ to $^2H_{11/2}$, $^4S_{3/2}$, $^4F_{9/2}$ and $^4I_{9/2}$ of Er^{3+}. A broad excitation band between 870 and 1,000 nm might be originating from the several transitions such as $^4I_{15/2}$–$^4I_{11/2}$, $^4I_{11/2}$–$^2H_{11/2}$, $^4I_{13/2}$–$^2F_{9/2}$, and $^2F_{9/2}$–$^2H_{9/2}$, which can explain why Er^{3+} ion could emit intense upconverted visible light when excited by 980 nm LD. In addition, the absorption band of Yb^{3+} ion is also located in this wavelength region, which provides a basic proof of energy

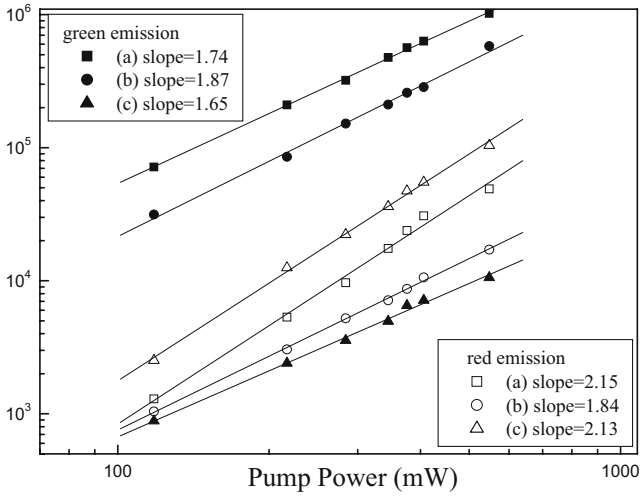

Fig. 6 Dependence of upconversion emission intensity of (*a*) monoclinic $Gd_2(MoO_4)_3$, (*b*) orthorhombic $Gd_2(MoO_4)_3$, (*c*) monoclinic Gd_2MoO_6 on pump laser power

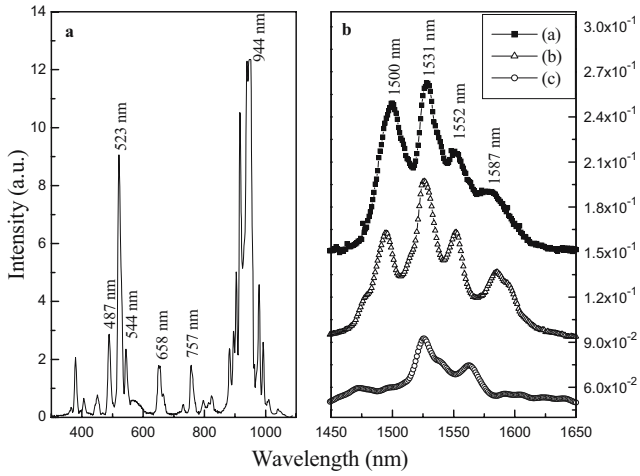

Fig. 7 **a** excitation (λem=1,530 nm) spectra of monoclinic $Gd_{1.78}Yb_{0.2}Er_{0.02}$ $(MoO_4)_3$ and **b** IR emission spectra (λex=980 nm with 47 mW of excitation power) of Er^{3+} and Yb^{3+} codoped (*a*) monoclinic $Gd_2(MoO_4)_3$, (*b*) orthorhombic $Gd_2(MoO_4)_3$, (*c*) monoclinic Gd_2MoO_6 nanocrystals

transferring from Yb^{3+} ion to Er^{3+} ion. A broad emission band presented at the wavelength from 1,450 to 1,650 nm is attributed to the radiative transition from excited state $^4I_{13/2}$ to ground state $^4I_{15/2}$ of Er^{3+} when pumped at 980 nm as a consequence of the non-radiative relaxation from higher energy states. The radiative transition $^4I_{13/2}$–$^4I_{15/2}$ in Er^{3+} and Yb^{3+} codoped gadolinium molybdates are split into four peaks by crystal field, and which show some differences in these samples.

Dopant concentration effects

The influence of dopant concentration on both down-conversion infrared and upconversion visible luminescence of m-G1-YE excited by 980 nm LD with 38 mW excitation power upon are investigated as shown in Fig. 8 and Fig. 9. The experimental conditions such as excitation power and detectors are identical for all the samples. The value of emission intensity is calculated by the integer of an energy range. The luminescence is enhanced by increasing the concentration of Er^{3+} for an interactive energy transfer (ET) to take place between the neighboring Er^{3+} ions as explained below:

$$Er^{3+}\left(^4I_{11/2}\right) + Er^{3+}\left(^4I_{13/2}\right) \rightarrow Er^{3+}\left(^4I_{15/2}\right) + Er^{3+}\left(^2F_{9/2}\right)$$

$$Er^{3+}\left(^4I_{11/2}\right) + Er^{3+}\left(^4I_{11/2}\right) \rightarrow Er^{3+}\left(^4I_{15/2}\right) + Er^{3+}\left(^2F_{7/2}\right)$$

The maximum luminescence intensity is achieved when the concentration of Er^{3+} arrives at 2 mol% of Gd^{3+}. Both probability of energy transfer among neighboring Er^{3+} ions,

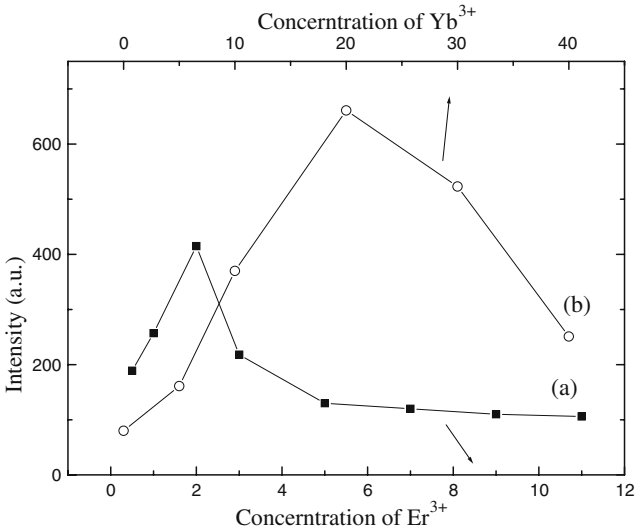

Fig. 8 The intensity of upconversion luminescence emission excited by 980 nm LD with 38 mW excitation power upon the concentration of (*a*) Er^{3+} (mol% of Gd^{3+}) and (*b*) Yb^{3+} (mol% of Gd^{3+}) in m-$Gd_2(MoO_4)_3$, the concentration of Yb^{3+} was kept at 10 mol% of Gd^{3+} in samples of (*a*) curve and that of Er^{3+} was kept at 2 mol% of Gd^{3+} in those of (*b*)

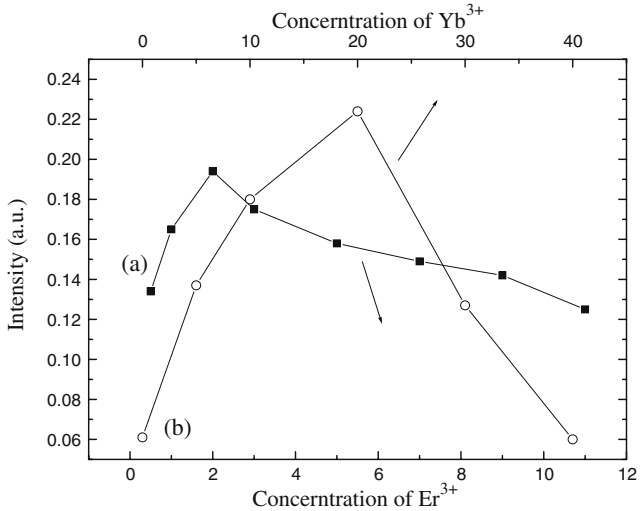

Fig. 9 The intensity of infrared emission excited by 980 nm LD with 38 mW excitation power upon the concentration of (*a*) Er^{3+} (mol% of Gd^{3+}) and (*b*) Yb^{3+} (mol% of Gd^{3+}) in m-$Gd_2(MoO_4)_3$, the concentration of Yb^{3+} was kept at 10 mol% of Gd^{3+} in samples of (*a*) curve and that of Er^{3+} was kept at 2 mol% of Gd^{3+} in those of (*b*)

where Er^{3+} ions in proximity are coupled by a MRP process in which one ion returns to the ground state and the other is excited to an upper level, and the UL centers increase with the concentration of Er^{3+} increasing. However, concentration-quenching affect becomes a predominant factor leading to a decrease in the luminescence intensity while the concentration of Er^{3+} is higher than 2 mol% of Gd^{3+}.

Yb^{3+} ion is frequently used as a sensitizing ion to increase the UL of the Er^{3+} ion for energy matching of the gap (between $^2F_{7/2}$ and $^2F_{5/2}$) of Yb^{3+}, and the excitation wavelength at 980 nm as illustrated in Fig. 10. One photon promotes Yb^{3+} ion from $^2F_{7/2}$ to $^2F_{5/2}$ through GSA, and then transfers the energy to Er^{3+} ion and promotes it to a higher level through ET processes as illustrated here:

$$Yb^{3+}\left(^2F_{5/2}\right) + Er^{3+}\left(^4I_{15/2}\right) \rightarrow Er^{3+}\left(^4I_{11/2}\right) + Yb^{3+}\left(^2F_{7/2}\right)$$

$$Yb^{3+}\left(^2F_{5/2}\right) + Er^{3+}\left(^4I_{11/2}\right) \rightarrow Er^{3+}\left(^2F_{7/2}\right) + Yb^{3+}\left(^2F_{7/2}\right)$$

$$Yb^{3+}\left(^2F_{5/2}\right) + Er^{3+}\left(^4I_{13/2}\right) \rightarrow Er^{3+}\left(^4F_{9/2}\right) + Yb^{3+}\left(^2F_{7/2}\right)$$

The population in levels $^2H_{11/2}$, $^4S_{3/2}$, and $^4F_{9/2}$ of Er^{3+} are increased due to energy transfer from Yb^{3+}. The luminescent intensity of m-G1-YE is much higher than that of m-G1-E, and it arrives at maximum when the doping concentration of Yb^{3+} is 20 mol% of Gd^{3+}. However, the luminescent intensity decreases when the concentration of Yb^{3+} is larger than 20 mol% of Gd^{3+}. Similar concentration quenching of dopant is observed in o-G1-YE and m-G2-YE.

With an overall comparison, it is found that the intensity of both the down-conversion and UL of Er^{3+} is much higher in m-G1-YE than o-G1-YE, which could possibly due to the lower structural symmetry of m-G1, and hence

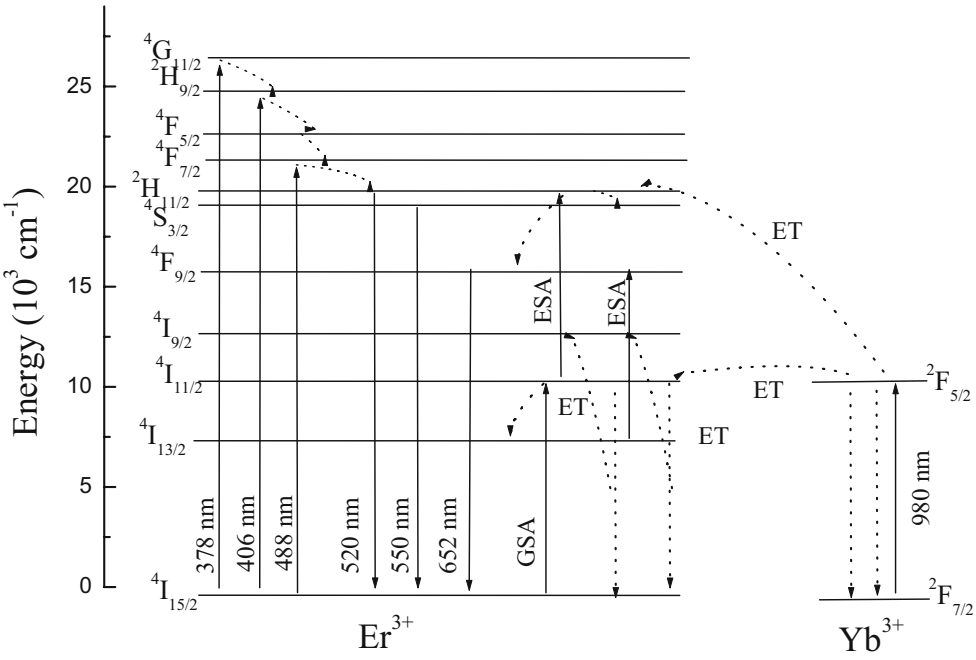

Fig. 10 Schematic energy level diagram of Er^{3+} and Yb^{3+} codoped gadolinium molybdates

the electronic transition is not so restricted by the parity selection rule in m-G1 as that in o-G1. Further, it has been found that the green UL of both m-G1-YE and o-G1-YE are bright enough to be observed by the naked eyes at a pump power as low as 38 mW and the emission slits kept at 0.1 nm.

Conclusion

We conclude that Er^{3+}/Yb^{3+}-codoped gadolinium molybdate nanocrystals $Gd_2(MoO_4)_3$ and Gd_2MoO_6 have been synthesized by the Pechini method with citric acid and ethylene glycol. Their structures and luminescence properties have been investigated. The average nanocrystals sizes are 50–70 nm. Phase transition from monoclinic to orthorhombic structure occurred while sintering the precursors of G1 at 726°C. Three intense emissions at 520, 550, and 650 nm have clearly been observed and the involved mechanisms have been explained. The green emissions at 520 and 550 nm are due to the transitions $^2H_{11/2}$–$^4I_{15/2}$ and $^4S_{3/2}$–$^4I_{15/2}$, respectively. The red upconversion emission at 650 nm is associated with the $^4F_{9/2}$–$^4I_{15/2}$ transitions of Er^{3+} ions. The quadratic dependence of fluorescence on excitation laser power confirms that two-photons contribute to upconversion of the green and red emissions. It is interesting to notice that predominant green emissions have clearly been observed both in down-conversion and UL spectra of m-G1 and o-G1, whereas, the red emission has been more intense than the green emission in m-G2. The optimal dopant concentration of Er^{3+} and Yb^{3+} are 2 mol% and 20 mol% of Gd^{3+} in m-G1, respectively. The novelty of this optical material has been its promising optical properties, which strongly encourage their further development as the rare-earth doped UL nanocrystals for biological labels.

Acknowledgements This work is jointly supported by NSFC (Grant No. 50472053), NCET (Grant No. 04-0823), YNSF (Grant No. E5050680) and China Postdoctoral Science Foundation (20060390200). We are grateful to Mr. C.H. Yang and Mr. G. X. Cheng for helpful discussions and technical assistance.

References

1. Jia CJ, Sun LD, Luo F, Jiang XC, Wei LH, Yan CH (2004) Appl Phys Lett 84:5305
2. Riwotzki K, Haase M (1998) J Phys Chem B 102:10129
3. Wakefield G, Holland E, Dobson PJ, Hutchison JL (2001) Adv Mater 13:1557
4. Yu M, Lin J, Wang Z, Fu J, Wang S, Zhang HJ, Han YC (2002) Chem Mater 14:2224
5. Guo H, Dong N, Yin M, Zhang WP, Lou LR, Xia SD (2004) J Phys Chem B 108:19205
6. Lei YQ, Song HW, Yang LM, Yu LX, Liu ZX, Pan GH, Bai X, Fan LB (2005) J Chem Phys 123:174710
7. Vetrone F, Boyer JC, Capobianco JA, Speghini A, Bettinelli M (2003) Chem Mater 15:2737
8. Matsuura D (2002) Appl Phys Lett 81:4526
9. Rosa-Cruz E, Diaz-Torres LA, Rodriguez-Rojas RA, Meneses-Nava MA, Barbosa-Garcia O (2003) Appl Phys Lett 83:4903
10. Zhang QY, Feng ZM, Yang ZM, Jiang ZH (2006) J Quant Spectrosc Radiat Transfer 98:167
11. Yi GS, Lu HC, Zhao SY, Ge Y, Yang WJ, Chen DP, Guo LH (2004) Nano Lett 4:2191

12. Zeng JH, Su J, Li ZH, Ya RX, Li YD (2005) Adv Mater 17:2119
13. Tuan VD, Guy G (2003) Sens Actuators B 9:104
14. Bao JP, Xu XW, Fan HL, Mu QY, Li YP (2003) Mater Rev (in Chinese) 17:191
15. Sivakumar S, Diamente PR, Veggel van FCJM (2006) Chem Eur J 12:5878
16. Pechini MU (1967) US Patent No. 3330697
17. Liu W, Farrington GC, Chaput F, Dunn B (1996) J Electrochem Soc 143(3):879
18. Yi GS, Sun BQ, Yang FZ, Chen DP, Zhou YX, Cheng J (2002) Chem Mater 14:2910
19. Bubb DM, Cohen D, Qadri SB (2005) Appl Phys Lett 87:131909
20. Borchardt HJ, Bierstedt PE (1966) Appl Phys Lett 8:50
21. Shur YaV, Nikolaeva EV, Shishkin EI, Baturin IS, Shur AG, Utschig T, Schlegel T, Laupascu DC (2005) Appl Phys Lett 98:74106
22. Pan YX, Su Q, Xu HF, Chen TH, Ge WK, Yang CL, Wu MM (2003) J Solid State Chem 74:69
23. Evans JSO, Mary TA, Sleight AW (1997) J Solid State Chem 133:580
24. Pollnau M, Gamelin DR, Luthi SR, Gudel HU, Hehlen MP (2000) Phys Rev B 61:3337